Virologica Sinica 40 (2025) 477–490

Contents lists available at ScienceDirect

Virologica Sinica

journal homepage: www.keaipublishing.com/en/journals/virologica-sinica
www.virosin.org

Research Article

Clofazimine targeting the spike protein and RdRp exhibits highly efficient antiviral activity against porcine epidemic diarrhea virus *in vitro*

Shuting Zhou [a,b], Junrui Zhu [c], Houde Zhao [a,b], Zixin Huang [a,b], Kangqi Zheng [a,b], Fan Xia [d], Yufan Xu [a,b], Guocheng Zhao [a,b], Jijie Jiang [a,b], En Zhang [b], Haoyang Nian [b], Li Cui [b], Tao Sun [b], Xiangfeng Wang [d], Yanjun Zhou [c], Zhibiao Yang [a,b,*], Zhe Wang [a,b,*]

[a] *Shanghai Collaborative Innovation Center of Agri-Seeds / School of Agriculture and Biology, Shanghai Jiao Tong University, Shanghai, 200240, China*
[b] *Shanghai Key Laboratory of Veterinary Biotechnology, School of Agriculture and Biology, Shanghai Jiao Tong University, Shanghai, 200240, China*
[c] *Department of Swine Infectious Diseases, Shanghai Veterinary Research Institute, Chinese Academy of Agricultural Sciences, Shanghai, 200241, China*
[d] *College of Agronomy and Biotechnology, China Agricultural University, Beijing, 100094, China*

ARTICLE INFO

Keywords:
Porcine epidemic diarrhea virus (PEDV)
Clofazimine (CFZ)
Spike
RdRp
Inactivation

ABSTRACT

Porcine epidemic diarrhea virus (PEDV) infection causes acute watery diarrhea in neonatal piglets, leading to substantial economic losses within the pig farming industry. This study demonstrates that clofazimine (CFZ) significantly inhibits PEDV replication in a dose-dependent manner *in vitro*, with negligible cytotoxicity. Findings from our time-of-addition assays indicate that CFZ effectively disrupts multiple stages of the viral infection cycle. Using a CoV-RdRp-Gluc reporter system, we evaluated the potency of CFZ against PEDV RNA-dependent RNA polymerase (RdRp), and determined a low IC_{50} value of 0.1364 μM. Molecular docking studies further confirmed that CFZ has high binding affinity at the active sites of the spike protein and RdRp protein in PEDV. Transcriptome analysis of Vero E6 cells, with and without CFZ treatment, revealed a significant change in transcriptional activity at 8 h post-infection (hpi). Moreover, the simultaneous application of CFZ and nucleoside analogs showed enhanced the anti-PEDV effect of CFZ *in vitro*. Our study underscores the potential of CFZ as a viable therapeutic agent against PEDV.

INTRODUCTION

The coronavirus disease 2019 (COVID-19), which emerged globally in 2020, has brought coronaviruses back into the spotlight, posing a significant threat to global public health. Fortunately, since the emergence of the Omicron variant, the pathogenicity of the virus has gradually decreased (Wang et al., 2023b; Li et al., 2023a). Coronaviruses infect a wide range of animals and humans and primarily cause diseases in the respiratory and gastrointestinal tracts. A recent study revealed that both the Omicron and Delta variants of the SARS-CoV-2 have the ability to infect and replicate within brain tissues (Li et al., 2023b). Porcine epidemic diarrhea virus (PEDV) belongs to the *Alphacoronavirus* genus within the *Coronaviridae* family and is characterized as a single-stranded, positive-sense genomic RNA. It causes porcine epidemic diarrhea (PED)—a disease manifesting as vomiting, acute watery diarrhea, dehydration, and even death. PEDV has been the most predominant diarrheal virus of the past decade in China (Chen et al., 2019; He et al., Based on the homology of the S gene, PEDV can be categorized into two major genotypes (G1 and G2), which are further subdivided into subgroups: G1a/b and G2a/b/c/d. In 2014, the United States reported the "S-INDEL" strain, a recombination linage derived from G1 and G2 strains with higher genetic homology to G1. This strain is characterized by relatively low pathogenicity and lethality in lactating piglets. By contrast, the "non-S INDEL" strain, encompassing G2a and G2b subtypes, is accountable for the ongoing global PED pandemic. Thus, current strategies for managing PEDV primarily rely on improved feeding management and effective biosecurity measures established in affected regions (Li et al., 2023c).

China has made significant strides in vaccine development (Wang et al., 2023a), employing three bi- or tri-valent inactivated and live attenuated vaccines derived from the CV777 strain and introducing an

* Corresponding authors.
E-mail addresses: zbyang@sjtu.edu.cn (Z. Yang), wangz@sjtu.edu.cn (Z. Wang).

https://doi.org/10.1016/j.virs.2025.05.012
Received 14 September 2024; Accepted 28 May 2025
Available online 1 June 2025

attenuated bivalent vaccine from the G2a genotype (Li et al., 2020). Despite these advancements, the continuous evolution of PEDV necessitates the development of experimental vaccines tailored to the current epidemic strains and evaluation of the long-term effectiveness of preexisting vaccines. Additionally, the development of antiviral drugs is attaining increased interest (Guo et al., 2023; Yang et al., 2023). Coronavirus' structural and non-structural proteins (Li et al., 2021; Wu et al., 2023; Zhai et al., 2023), which orchestrate virus replication, transcription, translation, and virus-host cell interactions, serve as potential drug targets, including the spike protein and the RNA-dependent RNA polymerase (RdRp). The PEDV spike protein, crucial for receptor recognition and membrane fusion processes, is under intensive study for the development of therapeutic strategies (Xu et al., 2023; Zhang et al., 2020). The S2 fusion region is relatively conserved, making it a potential target for antiviral drug design (Huang et al., 2020). Previous studies have shown that the *S* gene is the necessary determinant for the virulence of PEDV (Peng et al., 2023; Wang et al., 2018). The spike protein was also critical for PEDV cell adaptation (Chen et al., 2023) and served as a primary target for potent neutralizing antibodies (Li et al., 2017). RdRp is an enzyme crucial for RNA virus replication. Due to its robust evolutionary stability, RdRp has emerged as a potential drug target, with several drugs, including remdesivir (Huang et al., 2023a; Xie et al., 2021), molnupiravir (Huang et al., 2023b), shown to inhibit PEDV proliferation *in vitro*. The binding of drugs to the amino acid residues of RdRp blocks the access of substrates and divalent cations to the central active site, thus inhibiting the enzyme's catalytic function and halting RNA replication.

Over recent years, several research groups, including ours, have provided evidence that the energy metabolism pathway can serve as an innovative target for anti-tuberculosis drug development (Bald et al., 2017; Wang et al., 2019). Clofazimine (CFZ), initially developed to treat drug-resistant tuberculosis and various other infections (Lin et al., 2022; Mirnejad et al., 2018; Zhang et al., 2017), operates primarily by interference with cellular energy metabolism (Cholo et al., 2012). Interestingly, CFZ has demonstrated effectiveness against RNA viruses, as substantiated by recent studies showing its potential to block membrane fusion facilitated by SARS-CoV-2's spike protein and inhibit the viral helicase's function (Yuan et al., 2021). Moreover, it has shown efficacy during the membrane fusion phase of rabies virus infection (Wu et al., 2021), and demonstrated the ability to target the RdRp of the virus, thereby inhibiting virus replication (Fernandes et al., 2021). However, despite the expanding knowledge of antiviral targets for coronaviruses, exploration into CFZ's role in impeding PEDV replication remains insufficient, warranting further research.

In this study, we report for the first time that CFZ exhibits an inhibitory effect against PEDV infection *in vitro*. We noted that CFZ effectively suppressed PEDV infection in Vero E6, porcine kidney epithelial cells (LLC-PK1), and intestinal porcine epithelial cells (IPEC-J2) without manifesting cytotoxicity. Moreover, it disrupted multiple stages of the PEDV life cycle, including viral adsorption, internalization and replication. Specifically, CFZ exhibits substantial inhibition of PEDV RdRp. Furthermore, it demonstrated a robust binding affinity for the active sites of the PEDV spike protein and resulting in the inactivation of the virus.

RESULTS

CFZ inhibits PEDV infection *in vitro*

To evaluate the efficacy of CFZ in inhibiting PEDV infection, Vero E6, LLC-PK1, and IPEC-J2 cells were seeded into 12-well plates. Once cellular confluence rate reached 90 %–100 %, the cells were infected with PEDV *SHpd2012* strain (0.1 MOI, multiplicity of infection) for 1 h. Subsequently, Vero E6 cells were exposed to fresh maintenance medium containing CFZ at varying concentrations from 0.625 to 10 μM, while LLC-PK1, IPEC-J2 cells were exposed to CFZ at varying concentrations from 0.32 to 10 μM, or DMSO. After 10 h post-infection, the infected cells were assessed to calculate the inhibition rate via cytopathic effect (CPE) and immunofluorescence assay (IFA) (Fig. 1A–D). Compared with the control group, CFZ treated cells produced insignificant CPEs and displayed lower specific green fluorescence with the increasing CFZ concentration. The CCK-8 assay measured Vero E6, LLC-PK1, and IPEC-J2 cells' viability across a range of CFZ concentrations, namely 0.16, 0.32, 0.625, 1.25, 5, 10, 40, 80, 160, and 320 μM. Supplementary Fig. S1A–C illustrates that the CC_{50} value for CFZ was 168.8 μM (Vero E6 cells), 276.5 μM (LLC-PK1 cells), and 354.1 μM (IPEC-J2 cells. The selection index (SI: the ratio of CC_{50} to IC_{50}) values were 745.25 (Vero E6), 606.23 (LLC-PK1), and 3747.49 (IPEC-J2), respectively (Table 1).

In parallel, virus titers of PEDV were also identified in the Vero E6 cells post CFZ incubation. Compared to the control group, the virus titers showed a progressive decrease with the increasing concentrations of CFZ (Fig. 1E).

The impact of CFZ on the replication of PEDV in both Vero E6, LLC-PK1, and IPEC-J2 cells was also analyzed using RT-qPCR assays at 10 hpi. Consistent with previous results, a reduction in PEDV genomic RNA was observed in all cell lines with increase in CFZ concentrations (Fig. 1F–H).

For a more comprehensive understanding of CFZ's inhibitory effect on PEDV, the expression level of the PEDV N protein in infected cells was assessed through Western blot assays at 10 hpi (Fig. 1I–K). Vero E6, LLC-PK1 and IPEC-J2 infected samples exhibited a dose-dependent decrease in PEDV N protein expression upon CFZ treatment. Interestingly, CFZ has a more significant antiviral effect on LLC-PK1 cells than on other cell types under the same conditions. In conclusion, these findings strongly suggest that CFZ could robustly inhibit PEDV replication *in vitro*.

The antiviral effect of CFZ on different infection stages of PEDV

To ascertain the stage at which CFZ targets the viral replication cycle, a time-of-addition assay was conducted on Vero E6 cells. Cells were infected with PEDV *SHpd2012* strain (MOI = 0.1), and 10 μM CFZ was added at different time points during the experiment (Fig. 2A). As shown in Fig. 2B and C, CFZ can block PEDV infection at all stages of virus infection. In addition, Western blot analysis (Fig. 2D) confirmed that the expression level of the N protein was drastically reduced at every stage of infection. The preceding data indicates that CFZ curtails PEDV infection by both thwarting viral entry and obstructing post-entry step.

The impact of CFZ on the PEDV infection cycle was further investigated by measuring virus titer using $TCID_{50}$ and PEDV *N* gene mRNA levels using RT-qPCR. This analysis determined the effects of CFZ on viral attachment, internalization, replication, and release. Initially, the effect of CFZ on the virus binding or entry was examined. Vero E6 cells were pretreated with 10 μM CFZ or DMSO at 37 °C for 1 h, followed by incubation with PEDV for 15 min and 1 h at 4 °C to allow virus absorption. The efficiency of viral adsorption was assessed using $TCID_{50}$ and RT-qPCR, illustrating that CFZ minimally affected viral particle adsorption (Fig. 3A). In the internalization assay, CFZ treatment caused a significant reduction in $TCID_{50}$ and PEDV *N* mRNA levels compared to DMSO, suggesting that CFZ likely inhibits PEDV internalization (Fig. 3B). Next, the impact of CFZ on PEDV replication was evaluated by introducing CFZ during the replication phase. As depicted in Fig. 3C, CFZ treatment led to a 1–3 log reduction of virus titers and a nearly two to tenfold decline in PEDV *N* mRNA levels in comparison to DMSO treatment. Furthermore, a marked reduction in PEDV-N-specific immunofluorescence was observed in cells treated with CFZ during the viral replication stage compared to the control (Supplementary Fig. S2A). Western blot analysis confirmed that CFZ inhibited PEDV N protein synthesis, suggesting that CFZ impedes PEDV replication (Supplementary Fig. S2B). Finally, the viral release assay indicated no significant difference in PEDV genomic RNA levels in the supernatants between CFZ and DMSO treatments (Fig. 3D).

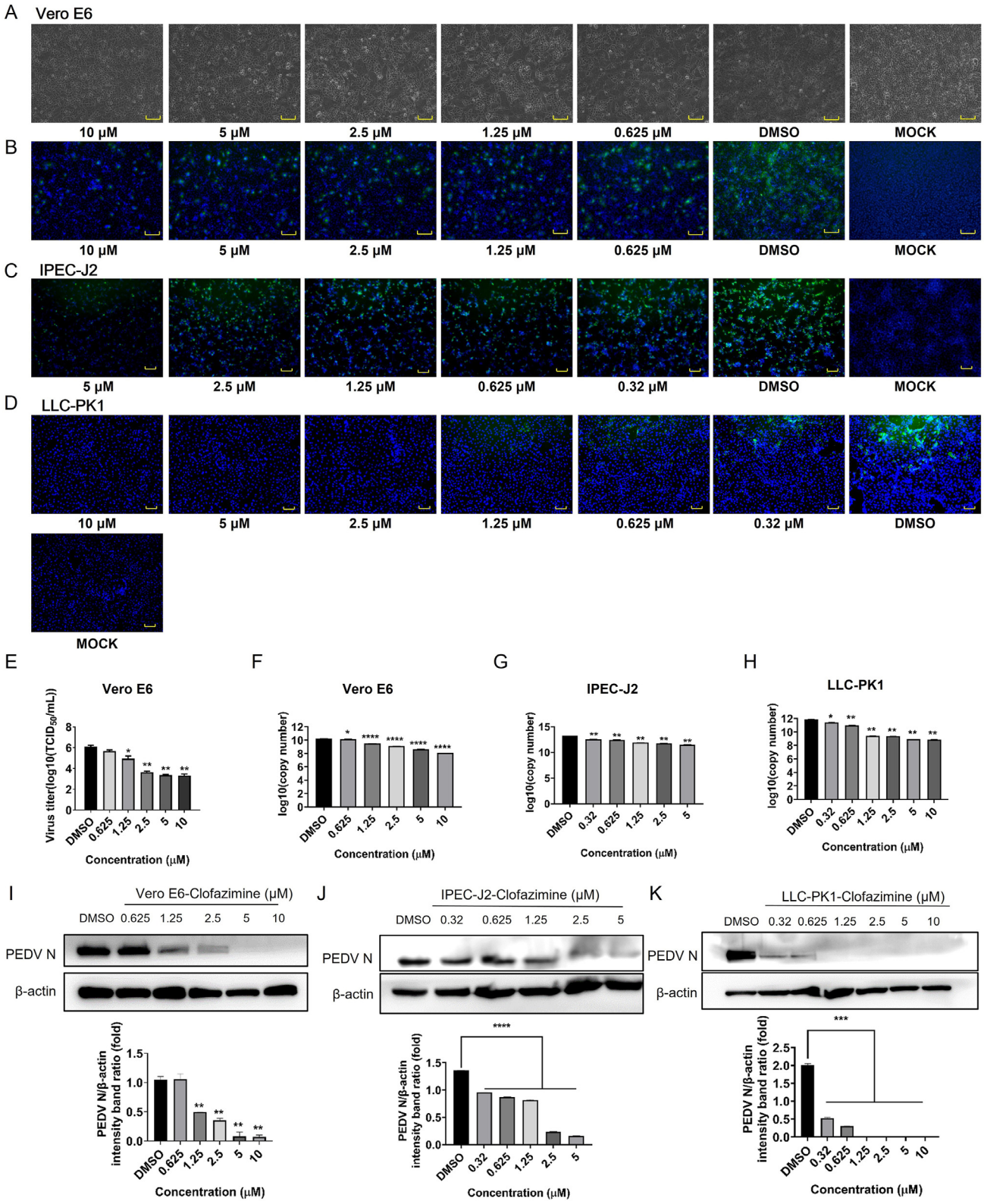

Fig. 1. Clofazimine (CFZ) inhibits PEDV infection *in vitro*. **A–D** Vero E6 cells (**A, B**), IPEC-J2 (**C**) cells, and LLC-PK1 cells (**D**) were treated with CFZ or DMSO and then infected with PEDV *SHpd2012* strain at an MOI of 0.1. The cytopathic effect was observed at 10 hpi (**A**). Cells were tested by immunofluorescence assay using a mAb against PEDV N protein. Scale bar = 100 μm. **E** The cell supernatants from PEDV-infected Vero E6 cells were collected at 10 hpi and titrated with a $TCID_{50}$ infectivity assay. **F–H** The PEDV genomic RNA in CFZ or DMSO treated Vero E6 cells (**F**), IPEC-J2 cells (**G**), and LLC-PK1 cells (**H**) were determined with RT-qPCR targeting the PEDV *N* gene. **I–K** Expression of the N protein in CFZ or DMSO treated Vero E6 cells (**I**), IPEC-J2 cells (**J**), and LLC-PK1 cells (**K**) was detected by Western blot. Asterisk (*) indicates a significant difference between CFZ and DMSO (*$P < 0.05$; **$P < 0.01$; ***$P < 0.001$; ****$P < 0.0001$).

Table 1
Selectivity index (SI) of clofazimine against PEDV *SHpd2012* strain in different cell lines. The IC50 was determined by a best-fit Log(dose)-response curve-fitting.

Cell lines	CC_{50} (μM)	IC_{50} (μM)	SI
Vero E6	168.8	0.2265	745.25
LLC-PK1	276.5	0.4561	606.23
IPEC-J2	354.1	0.09449	3747.49

CFZ inhibits the activity of PEDV RdRp

Because CFZ strongly inhibits the replication of PEDV, and given the crucial role of the coronavirus 3CLpro (Nsp5) and RdRp (also named Nsp12) in the replication and transcription process, we investigated CFZ's ability to inhibit the activity of 3CLpro and RdRp. Using fluorescence resonance energy transfer (FRET) assays, we found that clofazimine does not inhibit the activity of 3CLpro (Supplementary Fig. S3). To determine if CFZ could inhibit the replication of PEDV by targeting RdRp, an essential enzyme for RNA replication, we utilized an *in vitro* CoV-RdRp-Gluc reporter assay (Huang et al., 2023b). Initially, we successfully co-transfected 100 ng of PEDV-Gluc along with 1 μg of pcaggs-Nsp12-Flag (Fig. 4A), and the cytotoxic concentrations of CFZ were tested on HEK-293T cells (Supplementary Fig. S1D). At a concentration of 20 μM, CFZ significantly inhibited RdRp activity by approximately 100 % and exhibited an IC_{50} value of 0.1364 μM (Fig. 4B). RT-qPCR results further confirmated the inhibition of RdRp by CFZ (20 μM) (Fig. 4C). Molecular docking was employed to explore possible interactions between CFZ and the RdRp protein. The results identified a hydrogen bond with Arg175, and hydrophobic interactions with Leu168 and Ile172 for RdRp protein (Fig. 4D).

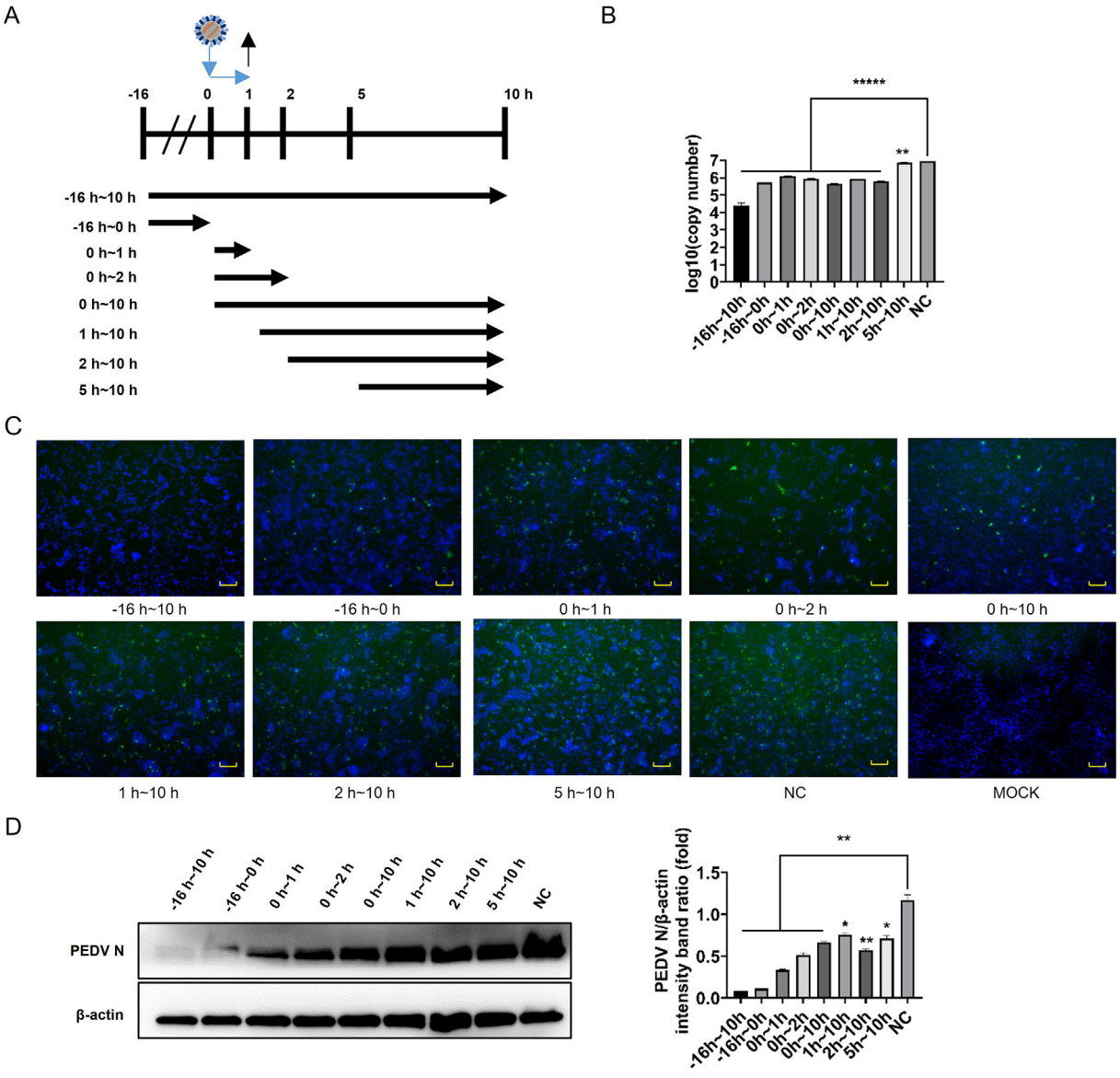

Fig. 2. Time-of-drug addition study of clofazimine (CFZ) treatment on PEDV infections. **A** Schematic illustration of the time-of-addition experiment. Vero E6 were infected with PEDV at an MOI of 0.1 and treated with CFZ (10 μM) at indicated time points. **B** The PEDV genomic RNA was determined by qPCR at 10 hpi. **C** Vero E6 cells were inoculated with PEDV *SHpd2012* at an MOI of 0.1 and treated with CFZ or DMSO at indicate time were tested with an IFA using a mAb to PEDV N protein. Scale bar = 100 μm. **D** Expression of the N protein was detected by Western blot at 10 hpi. NC denotes the DMSO-treated and infected group, while MOCK refers to the uninfected control group.

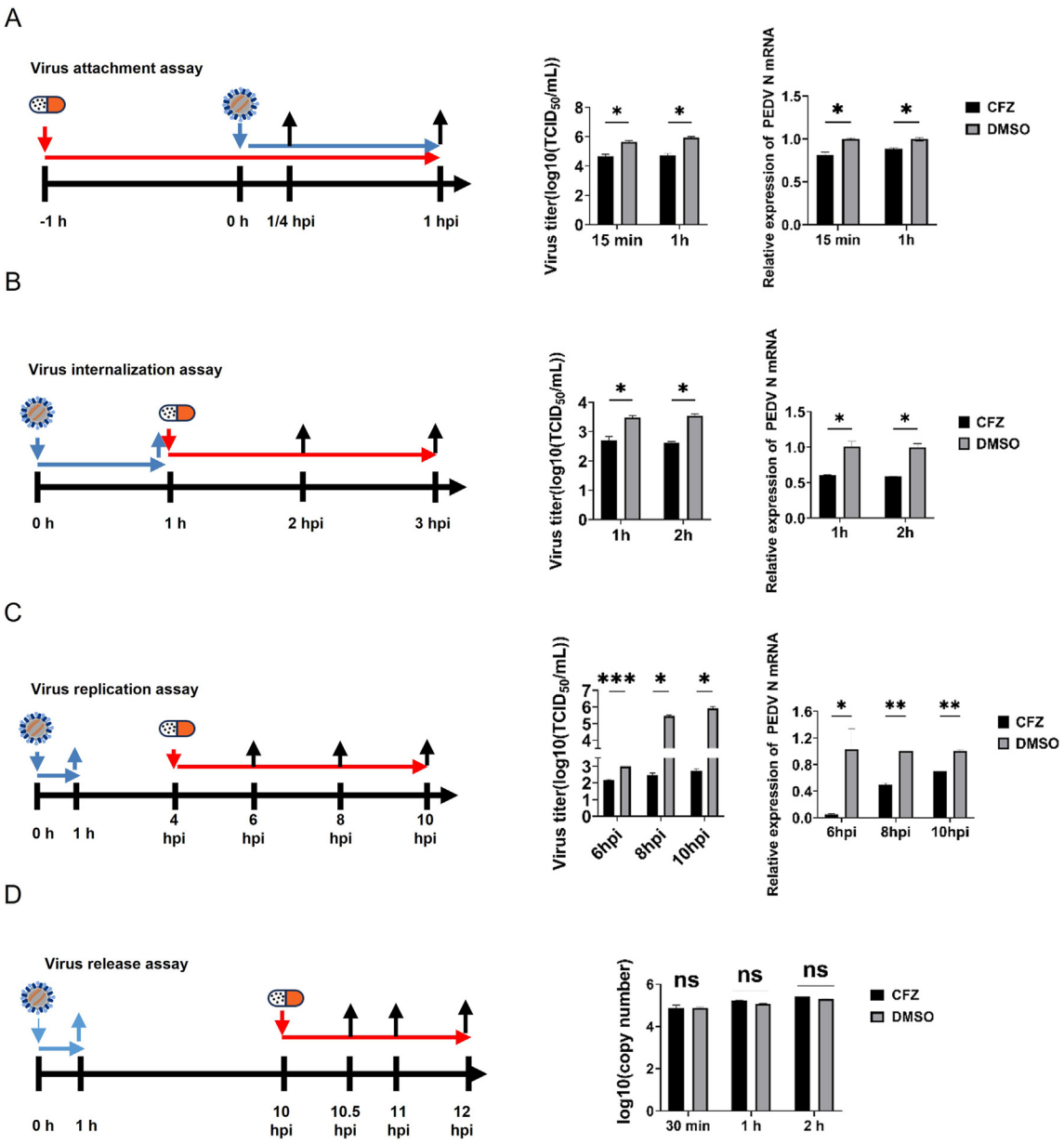

Fig. 3. The antiviral effect of clofazimine (CFZ) treatment on different infection stages of PEDV. **A–D** Vero E6 cells were infected with PEDV *SHpd2012* (MOI = 0.1) and treated with 10 μM CFZ at indicated time points, which represented the stage of viral attachment (**A**), internalization (**B**), replication (**C**) or release (**D**), respectively. At indicated time points, the samples were prepared for determining progeny virus titer by $TCID_{50}$ assay and determining PEDV *N* mRNA level by RT-qPCR.

CFZ inactivates PEDV virions directly

We investigated whether CFZ could directly inactivate the PEDV virus. The live PEDV virus was pre-treated with CFZ at 37 °C for various durations (15 min, 30 min, 1 h, 3 h, and 5 h) before inoculation into Vero E6 cells. Viral infectivity was assessed using RT-qPCR. As depicted in Fig. 5A, a significant reduction in virus infectivity was observed, suggesting that CFZ's inhibitory effect might partly result from its direct inactivation of PEDV virion particles. Another study was conducted to determine if CFZ leads to the degradation of the RBD domain. CFZ, at concentrations of 10 μM, was incubated with pcoldTF-RBD protein at 37 °C for 1 h or 3 h, followed by SDS-PAGE analysis. Results demonstrated that CFZ did not directly degrade the RBD protein as compared with the control (Fig. 5B). Transmission electron microscopy (TEM) was used to analyze PEDV morphology with or without 10 μM CFZ treatment. As shown in Fig. 5C, CFZ did not disrupt virion integrity, whereas the positive (Triton X-100 treatment) significantly compromised viral structure. Molecular docking was employed to explore possible interactions between CFZ and the spike protein, identifying a hydrogen bond with Ser488 and hydrophobic interactions with Val274, Gln470, Ser474, and Thr824 (Fig. 5D). Collectively, these data suggest that CFZ may interact with the viral spike protein to inactivate PEDV particles, although the precise molecular mechanism remains to be elucidated.

Antiviral activity of CFZ against different genotypes of PEDV strains

PEDV is classified into three major genotypes based on the spike gene sequence: G1 (classical), G2 (variant), and S-INDEL (characterized by nucleotide insertions/deletions in the *S* gene). Given that CFZ exhibits significant antiviral activity against the PEDV G2 strain (*SHpd2012*), we further investigated the anti-PEDV efficacy of CFZ against classical (G1

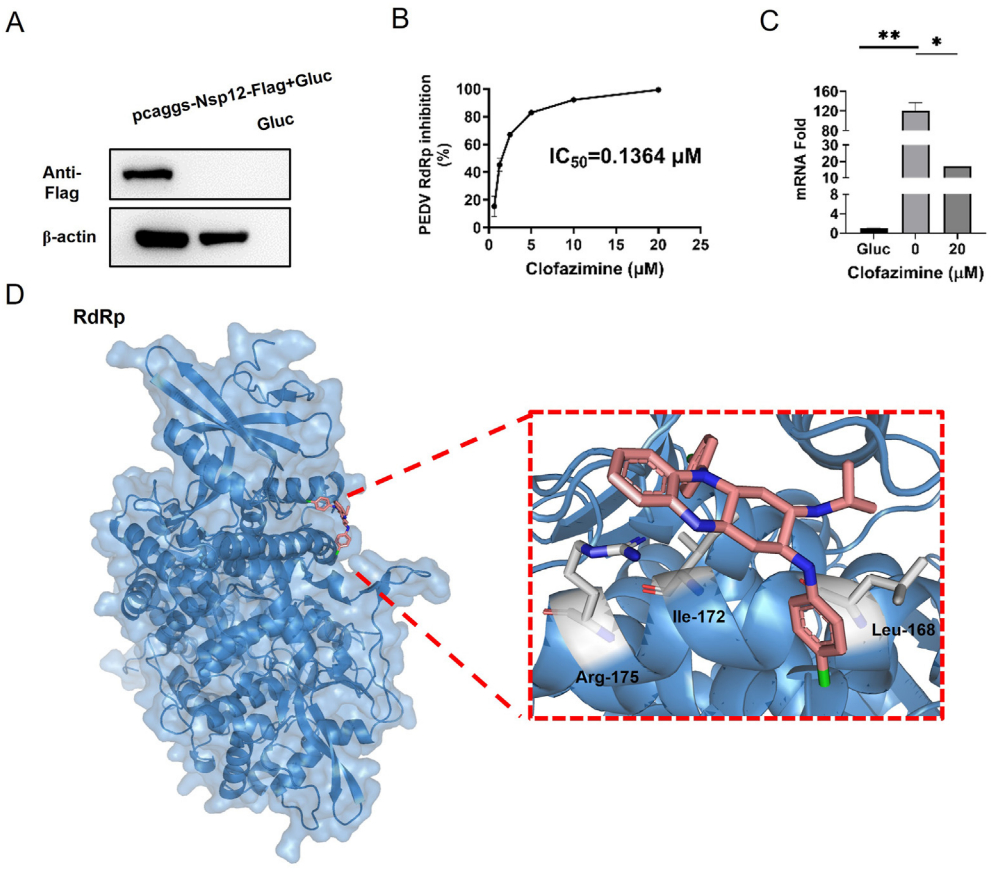

Fig. 4. Clofazimine (CFZ) inhibit PEDV RdRp activity. The HEK-293T cells were transfected with PEDV-Gluc and Nsp12 plasmid. Six hours post-transfection, cells were cultured with serially diluted CFZ. **A** Expression of the PEDV *Nsp12* (RdRp) gene was detected with an anti-Flag antibody by Western blot 24 h after transfection. **B** Dose-response curve of CFZ against PEDV-Gluc. **C** CFZ inhibited PEDV *RdRp* mRNA level. HEK-293T cells transfected with specified plasmids and treated with 20 μM CFZ. Then the cells were subjected to RT-qPCR to quantify Gluc mRNA levels. **D** Docking pose of CFZ in *SHpd2012* RdRp.

subtype: HLJ) and S-INDEL (AH2018) PEDV strains. Vero E6, LLC-PK, and IPEC-J2 cells were infected with classical (G1 subtype: HLJ) and S-INDEL (AH2018) PEDV strains, then treated with CFZ at different concentrations and harvested for determination of PEDV genomic RNA and protein expression. Cells were fixed and analyzed using IFA assays. RT-qPCR results showed that CFZ significantly suppressed PEDV genomic RNA of both genotypes in a dose-dependent manner compared to the control group across all three cell types (Fig. 6A–F). Subsequently, Western blot analysis revealed that CFZ treatment significantly decreased PEDV N protein synthesis in a dose-dependent manner (Fig. 6G–L). Notably, CFZ exhibited a more pronounced antiviral effect on G1 strain (HLJ) than S-INDEL strain (AH2018) under the same conditions in Vero E6 cells. Finally, IFA was conducted to detect the N protein expression in infected cells. PEDV-N-specific immunofluorescence gradually diminished with increasing concentrations of CFZ (Fig. 6M–R). Particularly, at a concentration of 10 μM, CFZ nearly blocked the PEDV-HLJ strain N protein synthesis in Vero E6 cells. In conclusion, these results indicate that CFZ could significantly inhibit viral genome replication and protein expression of both classical and S-INDEL PEDV strains in a dose-dependent manner. Likewise, similar antiviral effects were observed in IPEC-J2 and LLC-PK1 cells (Fig. 6).

Transcriptional analysis after CFZ treatment

To further explore the antiviral role of CFZ, we conducted RNA-seq analyses on Vero E6 cells infected with PEDV, both with and without CFZ treatment. The RNA-seq method was performed as previously described (Huang et al., 2023b). The Genome Sequence Archive (GSA: CRA013798), which contains the raw sequence data mentioned in this paper, has been deposited at the National Genomics Data Center in China. The samples were divided into four groups: 8h-CFZ, 8hpi-CFZ, 8hpi-DMSO, and MOCK. Our differential gene screening identified a total of 2508 differentially expressed genes (DEGs) between the MOCK and 8hpi-CFZ groups, compared to 4454 DEGs between the 8hpi-DMSO and 8hpi-CFZ groups (Fig. 7A, Supplementary Table S3). This suggests that CFZ significantly attenuates transcriptional changes at 8hpi.

For differential gene expression detection, we employed a $|\log2\text{-FoldChange}| > 1$, significant $P\text{-value} < 0.05$ as the screening criteria. Cluster analysis showed that the 8hpi-CFZ group clustered more closely with the MOCK group (Fig. 7B). PEDV infection notably activated the p53 signaling pathway, MAPK signaling pathway, and pentose phosphate pathway, all of which were attenuated by CFZ treatment (Fig. 7C). Gene Ontology (GO) analysis indicated that most of the top 20 significantly enriched GO terms belonged to the molecular function (MF) category, with terms related to ion binding, binding, and protein binding (Fig. 7D). Cellular component analysis revealed significant enrichment in terms related to membrane-bounded organelles and intracellular membrane-bounded organelles (Fig. 7D). From these results, we conclude that CFZ mitigates the transcriptional changes induced by PEDV infection in host cells.

Synergistic antiviral effects of CFZ combined with MOL and RDV

Remdesivir (RDV) and molnupiravir (MOL), as nucleotide analogs, exhibit anti-PEDV capabilities (Huang et al., 2023a, 2023b; Xie et al., 2021). The combined effects of clofazimine with either molnupiravir or

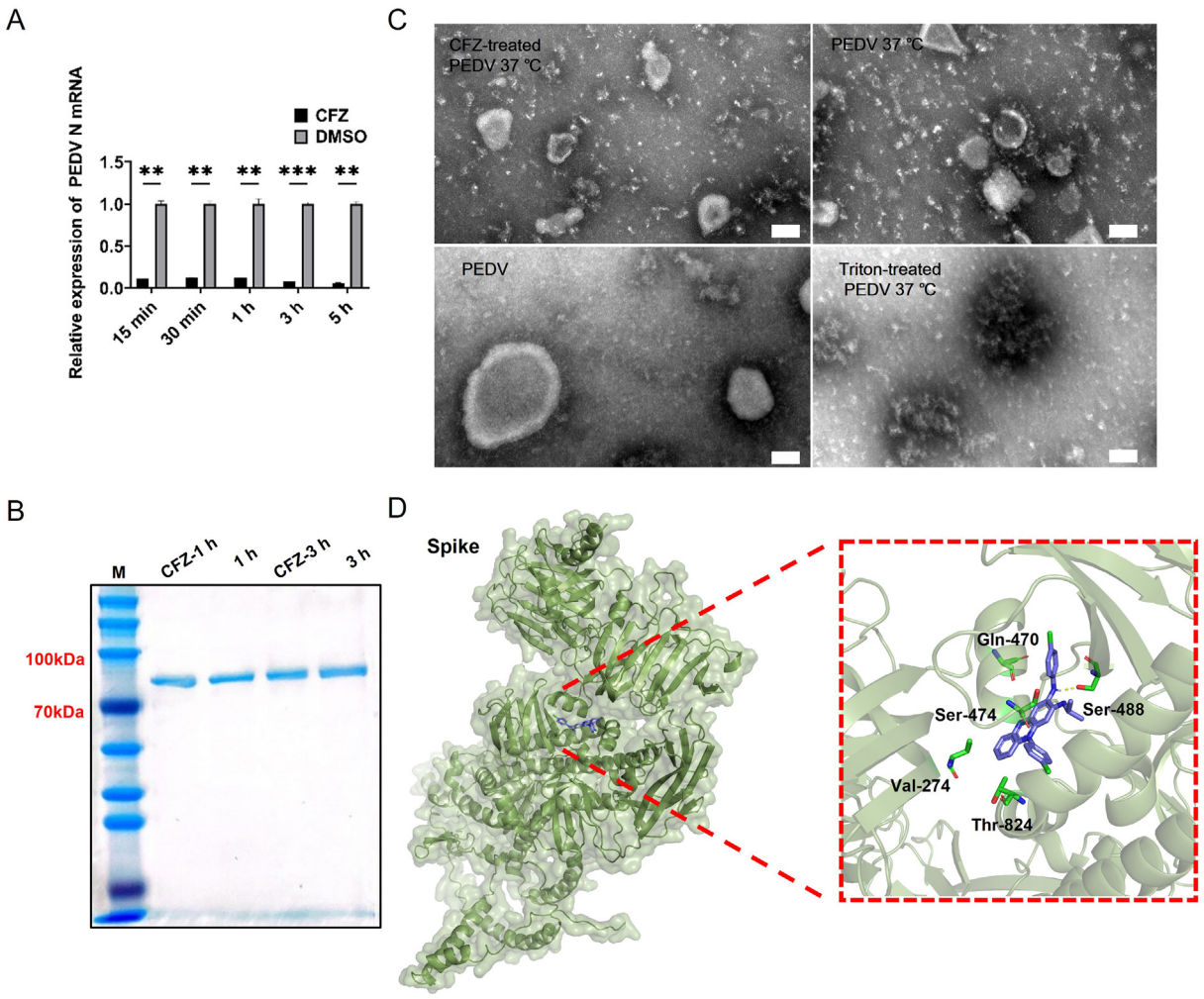

Fig. 5. Clofazimine (CFZ) inactivate virus particle. **A** CFZ (10 μM) was incubated with PEDV *SHpd2012* strain for 15 min, 30 min, 1 h, 3 h and 5 h at 37 °C, then the mixtures were added to Vero E6 cells. Cells were collected at 10 hpi and measured using RT-qPCR. **B** CFZ (10 μM) was incubated with pcoldTF-RBD for 1 h and 3 h at 37 °C, the degradation of RBD protein at the indicated times after treatment with CFZ was examined by SDS-PAGE analysis. **C** Morphology changes of PEDV with or without CFZ treatment. PEDV *SHpd2012* strain was incubated with CFZ (10 μM) or 0.01% Triton X-100 at 37 ℃ for 3 h. The morphology changes of viral particles were observed by transmission electron microscopy. Scale bars, 50 nm. **D** Docking pose of CFZ in *SHpd2012* spike.

remdesivir were subsequently examined. Initially, the cytotoxic concentrations of these compounds were tested on Vero E6 cells (Supplementary Fig. S4). Vero E6 cells were then infected with PEDV at an MOI of 0.1, treated with CFZ in combination with increasing doses of RDV and MOL, and incubated for 10 h. Synergistic efficacy was determined using RT-qPCR (Fig. 8A and B). To enhance antiviral efficacy, we evaluated the combined antiviral impacts of CFZ with either MOL or RDV through mathematical modeling using SynergyFinder. Our results indicate that CFZ concentrations ranging from 0.32 μM to 1.25 μM consistently demonstrate the highest synergistic effect with both RDV (Fig. 8C) and MOL (Fig. 8D) with negligible cytotoxicity. Overall, these findings suggest that CFZ combined with either RDV or MOL produces enhanced antiviral effects against PEDV infection.

DISCUSSION

PEDV leads to significant enteric disease, resulting in substantial economic losses for the global swine industry (Chen et al., 2019; He et al., 2022; Zhang et al., 2023). Due to the continuous emergence of variant PEDV strains, the protection offered by current vaccines proves to be inadequate. This situation warrants the development of more efficacious and safe vaccines and antiviral drugs. At present, a significant number of natural drugs have been proven effective against PEDV. Specifically, ethyl caffeate has been proven to target 3CLpro and inhibit PEDV replication (Jiang et al., 2025). Pinostrobin exhibit anti-PEDV activities by targeting PEDV fusion step (Chutiwitoonchai et al., 2025). Niclosamide inhibited PEDV infection by affecting viral internalization (Wang et al., 2023c). This paper represents an initial exploration into Clofazimine as a potent anti-PEDV drug, demonstrating anti-PEDV activity with an IC_{50} value of 0.1364 μM. Importantly, our study identified Clofazimine's significant inhibition of viral adsorption, internalization, and RNA-dependent RNA polymerase (RdRp) activity, and it significantly inhibited PEDV replication *in vitro*. Additionally, CFZ can directly inactivate viruses *in vitro*.

In our study, we observed that CFZ suppressed the production of PEDV (Fig. 1), demonstrating its recurring role in viral replication. CFZ can also inhibit the replication of the SARS-CoV-2 (Yuan et al., 2021), rabies virus (Wu et al., 2021) and Zika virus (Fernandes et al., 2021). The findings suggest that CFZ can obstruct PEDV adsorption, internalization, replication processes, and initiate direct inactivation of viruses. PEDV, a typical class I enveloped virus, uses the spike protein to facilitate the fusion of viral and host cell membranes, enabling its entry into host cells (Tang et al., 2020). It is noteworthy that CFZ has been reported to block potassium channels and further hindering viral membrane fusion (Leanza et al., 2014). It has been previously reported that CFZ curbs SARS-CoV-2 internalization by interfering with the spike protein (Yuan et al., 2021).

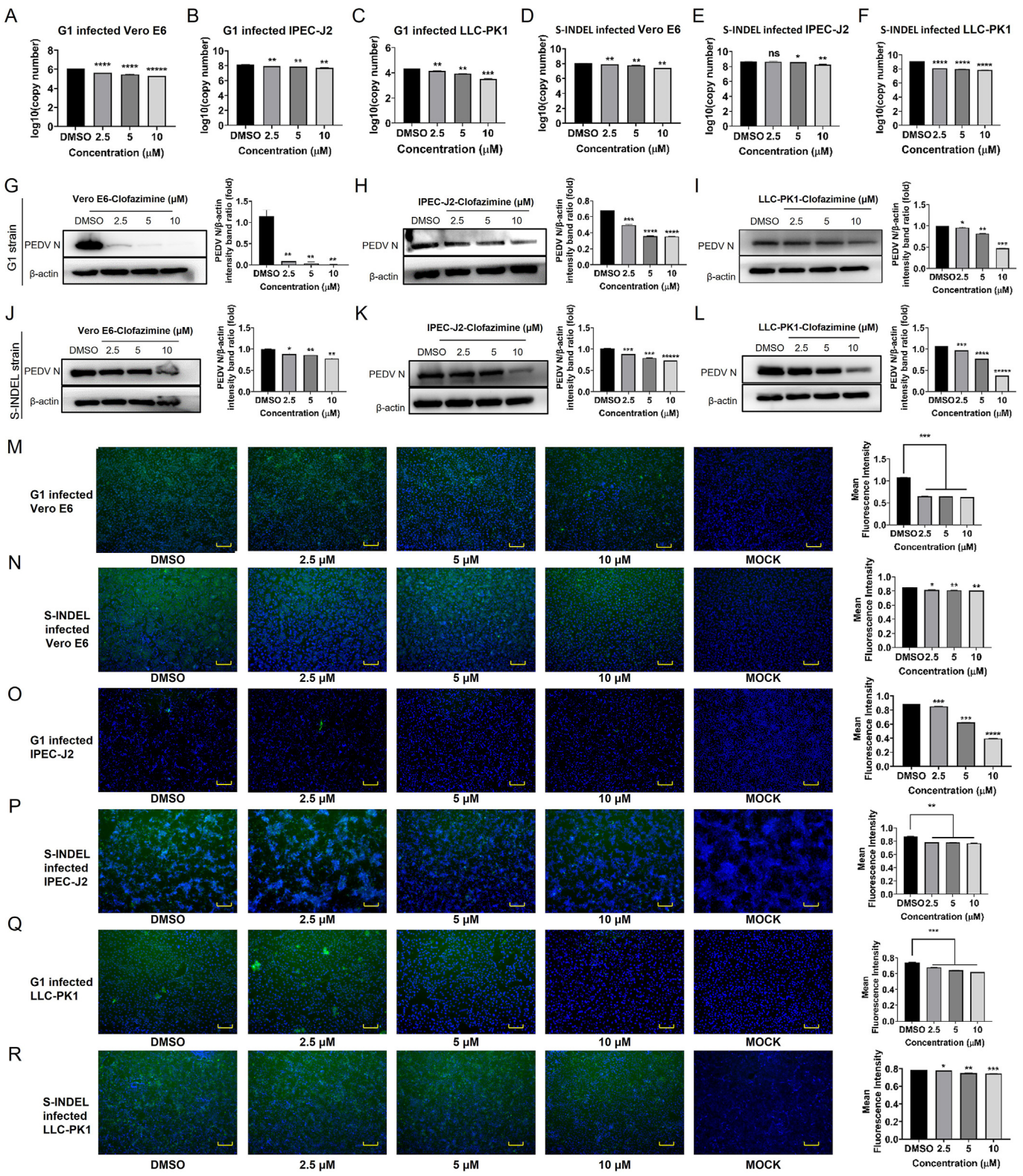

Fig. 6. Antiviral activity of clofazimine (CFZ) against different genotypes of PEDV strains at an MOI of 0.1 in Vero E6, IPEC-J2 and LLC-PK1 cells. **A–C** Effect of CFZ on viral RNA synthesis of PEDV G1 strain (HLJ) in Vero E6 (**A**), IPEC-J2 (**B**) and LLC-PK1 (**C**). **D–F** Effect of CFZ on viral RNA synthesis of PEDV S-INDEL strain (AH2018) in Vero E6 (**D**), IPEC-J2 (**E**) and LLC-PK1 (**F**). **G–I** Effect of CFZ on N protein expression of PEDV G1 strain by Western blotting in Vero E6 (**G**), IPEC-J2 (**H**) and LLC-PK1 (**I**). **J–L** Effect of CFZ on N protein expression of PEDV S-INDEL strain by Western blot in Vero E6 (**J**), IPEC-J2 (**K**) and LLC-PK1 (**L**). **M, N** PEDV N protein expression of G1 and S-INDEL strains in Vero E6 was determined by IFA. **O, P** PEDV N protein expression of G1 and S-INDEL in IPEC-J2 was determined by IFA. **Q, R** PEDV N protein expression of G1 and S-INDEL strains in LLC-PK1 cells was determined by IFA. Scale bars = 100 μm. MOCK refers to the DMSO-treated and uninfected group. The experiment was performed three times independently. Differences were considered significant at * $P < 0.05$, ** $P < 0.01$, *** $P < 0.001$, **** $P < 0.0001$.

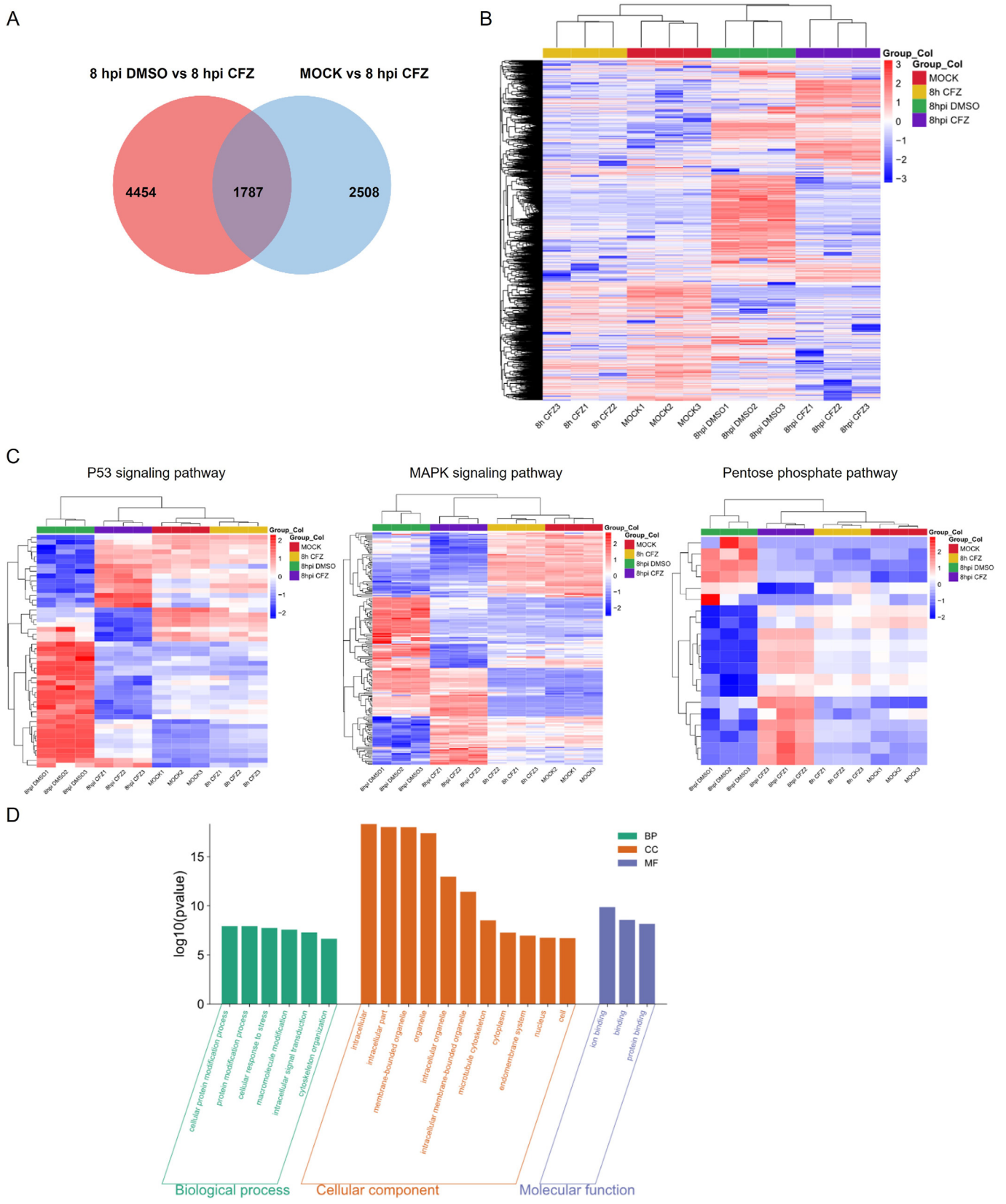

Fig. 7. Transcriptional analysis of clofazimine (CFZ) treatment. Vero E6 cells were infected with PEDV (MOI = 0.1) and treated with and without CFZ (10 μM). **A** Venn graph of differential expression gene. **B** Heat map and hierarchical clustering of the four groups. **C** Heat map across all samples enriched in p53 signaling, MAPK signaling and Pentose phosphate pathway. **D** The top 20 GO enrichments from group "8hpi DMSO vs 8hpi CFZ". BP, biological process. CC, cellular component. MF, molecular function. Expression difference multiple |log2FoldChange| > 1, significant *P-value* < 0.05.

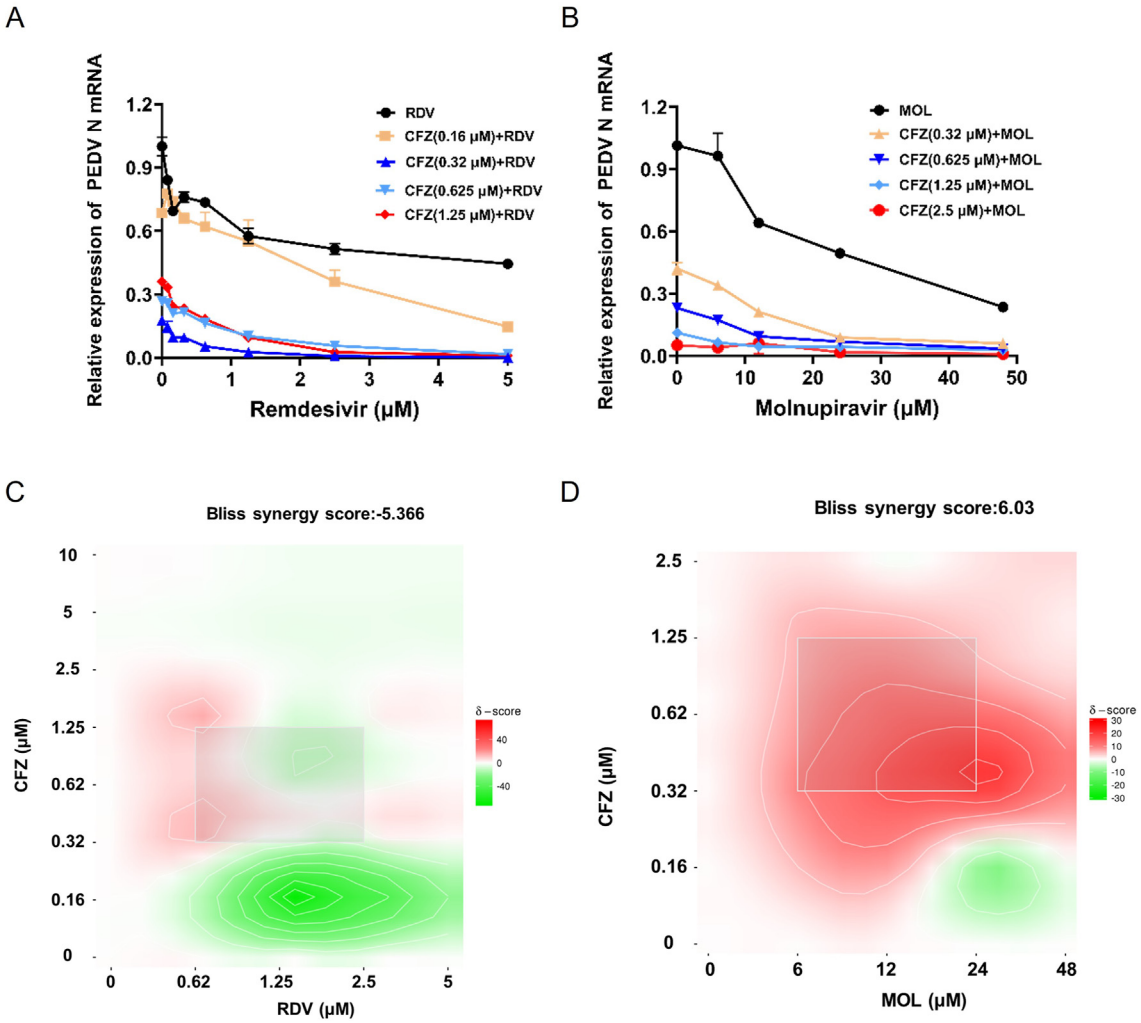

Fig. 8. Synergistic anti-PEDV efficacy of clofazimine (CFZ) with remdesivir or molnupiravir. **A, B** Vero E6 cells infected with PEDV, and then incubated with remdesivir (0.08 μM, 0.16 μM, 0.32 μM, 0.625 μM, 1.25 μM, 2.5 μM, 5 μM) or molnupiravir (6 μM, 12 μM, 24 μM, 48 μM) and CFZ, the cells were collect at 10 hpi and PEDV N mRNA were determined by RT-qPCR. **C, D** Two-dimensional topograph visualization of compound integration based on the Bliss synergy score that highlights the areas of synergy across the dose response matrix. The experiment was performed three times independently.

In this study, we observed that CFZ can inhibit PEDV internalization, in line with previous reports. Although we confirmed that CFZ could inhibit virus replication stage, we found that the inhibition of PEDV replication by CFZ differs from that of the SARS-CoV-2. It does not act by suppressing viral helicase activity but rather exhibits antiviral effects by dose-dependently inhibiting RdRp activity with negligible cytotoxicity. Developing new drugs often focuses on targeting the RdRp active site responsible for viral genome replication. Nucleotide analogs belong to a class of RdRp inhibitors, including remdesivir and molnupiravir. Remdesivir inhibits viral replication by allowing RdRp to use remdesivir as a substrate, which leads to the incorporation of remdesivir monophosphate (RMP) into RNA molecules. This incorporation causes RdRp to extend the RNA strand by three nucleotides, stopping transcription (Kokic et al., 2021). Molnupiravir is a biological prodrug of β-D-N (4)-hydroxycytidine (NHC). Molnupiravir's antiviral mechanism relies on RdRp using NHC triphosphate as a substrate instead of cytidine or uridine triphosphate, which can result in altered RNA products during synthesis (Kabinger et al., 2021). We found that CFZ, as a non-nucleoside analogue, exhibits synergistic antiviral effects with nucleoside analogs remdesivir and molnupiravir with negligible cytotoxicity. Although we have demonstrated the potential synergistic antiviral effects of CFZ with RDV and MOL, a significant amount of work is still needed to achieve its clinical application. Whether CFZ destroys the virus genome needs further explorations. Interestingly, CFZ can also directly inactivate PEDV virions *in vitro* with only 15 min of co-incubation, which has not been reported in previous studies on CFZ. Additionally, even though the S1-RBD protein is linked to virus attachment and entry, CFZ was unable to degrade the S1-RBD protein *in vitro*. Molecular docking analysis revealed that CFZ binds to the spike sites Val274, Gln470, Ser474, Ser488 and Thr824, leading us to speculate that CFZ might bring about its virus-inactivating effects by binding to the spike. Additionally, it is interestingly that CFZ has a more significant antiviral effect on PEDV G2 strain (*SHpd2012*) than that of G1(HLJ) and S-INDEL(AH2018) strains under the same conditions. CFZ nearly blocked the PEDV *SHpd2012* strain N protein synthesis in Vero E6 cells at a concentration of 5 μM and 1.25 μM for LLC-PK1 cells. Moreover, the anti-PEDV effect of CFZ on the G1 strain (HLJ) was more potent than that on S-INDEL strain (AH2018) in Vero E6 cells. In conclusion, this report presents for the first time, detailed insights into the potential inhibitory effects of CFZ against PEDV infections *in vitro*, operative across multiple stages. Taken together, these findings suggest that CFZ could potentially serve as an effective treatment for PEDV infection.

Transcriptome data analysis suggested that treatment with CFZ could result in partial restoration of the gene expression modifications instigated by PEDV infection in Vero E6 cells. Notably, CFZ treatment induced rejuvenation of the genes allied with three important pathways: p53

signaling, MAPK signaling, and the pentose phosphate pathway. Activation of the p53-regulated pathway potentially results in a cell cycle arrest, thereby inhibiting the impact of PEDV and similar viruses (Su et al., 2021). Furthermore, successful viral infection necessitates the activation of MAPK signaling (Wang et al., 2022). Interestingly, several viruses exploit the non-oxidative branch of the pentose phosphate pathway (PPP) for generating replication-essential nucleotides (Rashida Z, 2021). In our study, we found that CFZ has the potential to target viral proteins to suppress virus proliferation. Additionally, CFZ was found to hamper virus replication by mitigating the metabolic alterations in the host incited by the virus.

CONCLUSIONS

In this study, CFZ was identified as a PEDV inhibitor. CFZ may interfere with the virus proliferation process by simultaneously targeting the virus spike protein and RdRp, and can directly inactivate the virus *in vitro*, exhibiting potent antiviral activity (Fig. 9). This antiviral effects at multiple stages of the viral infection cycle have not been reported in previous anti-PEDV drugs. Our findings may contribute to novel drug design strategies to combat PEDV infection and may be extended to counter prevalent coronavirus infections.

MATERIALS AND METHODS

Cells, virus, antibodies and drugs

Vero E6, IPEC-J2, and HEK-293T cells were cultured in Dulbecco's Modified Eagle's Medium (DMEM) (GIBCO, USA) containing 10 % fetal bovine serum (Biological Industries, USA) at 37 °C with 5 % CO_2. LLC-PK1 were grown in Minimum Essential Medium (MEM, Gibco, USA) supplemented with 10 % inactivated fetal bovine serum (FBS) (Biological Industries, USA). All the cells were maintained in our laboratory.

The PEDV G2 strain *SHpd2012* (GenBank accession no. MN508818.1) was previously isolated in Vero E6 cells in our laboratory(Luo et al., 2020). PEDV G1 strain HLJ and "S-INDEL" strain AH2018 were generously provided by Professor Yanjun Zhou of Shanghai Veterinary Research Institute, CAAS. PEDV titers were determined by a 50 % tissue culture infective dose ($TCID_{50}$) assay in Vero E6 cells. The monoclonal antibody (mAb) against the PEDV N protein was made in our laboratory (Wang et al., 2016).

Anti-Flag mouse mAb was purchased from ABmart (M20008 M, Abmart, Shanghai, China), anti-β-actin mouse mAb was purchased from Genscript (A00702, Genscript, China). Goat Anti-Mouse IgG-HRP was purchased from ABmart (M21011, Abmart, Shanghai, China). FITC Goat Anti-Mouse IgG (H + L) was purchased from Shanghai Fushen Biotechnology Co.Ltd (FSM0059, FuShen, China). Clofazimine (R021340) and Remdesivir (R125975) were purchased from Rhawn (Shanghai, China). Molnupiravir (CAS no. 2492423-29-5) was purchased from MedChemExpress, USA (Monmouth Junction, NJ, USA). All the drugs were dissolved in DMSO (60313ES60, YEASEN, Shanghai, China) to make a stock solution (Supplementary Table S1).

Cytotoxicity assay

Cell viability of Vero E6, LLC-PK1, and IPEC-J2 cells was determined using commercial Cell Counting Kit-8 (CCK-8) (TOPSCIENCE, Shanghai, China) in accordance with the manufacturer's instructions. Briefly, cells were seeded on a 96-well plate and cultured for 24 h, followed by incubation with different doses of CFZ for an additional 24 h and then 10 μL of CCK-8 reagent was added to each well and incubated at 37 °C for 2 h. The CCK-8 signal was measured at an absorbance of OD_{450} nm. All assays were performed in triplicate. The relative viability of the cells was calculated as the percentage of the optical density relative to that of the control sample.

Inhibition of virus infection

Vero E6, LLC-PK1, and IPEC-J2 cells were infected with PEDV (MOI = 0.1) for 1 h at 37 °C. The virus solution was then discarded and the 12-well plate was washed twice with PBS. Fresh maintenance medium containing 10 μg/mL trypsin with or without different doses of CFZ was subsequently added. At 10 h post-infection (hpi), cells and cell culture supernatants were collected to determine the antiviral efficiency of the compounds on the cells.

$TCID_{50}$ assay

Vero E6 cells were seeded into a 96-well plate and incubated at 37 °C under an atmosphere of 5% CO_2. The supernatant was then removed, and monolayers of cells were washed twice with PBS. Then, 100 μL of 10-fold serial dilution of viral samples was added to each well. Each group was diluted in 8 duplicate wells and the cytopathic effect was examined every 24 h at 37 °C for 5 days post-inoculation. The PEDV titer was calculated in accordance with the Reed and Muench method.

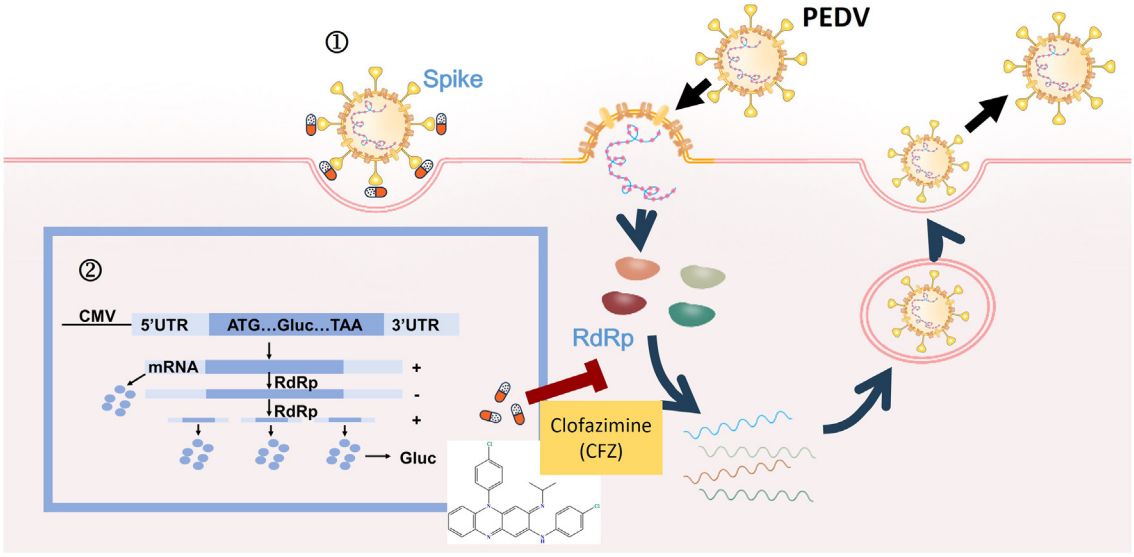

Fig. 9. Graphical abstract. ① clofazimine (CFZ) inhibits spike-mediated membrane fusion. ② CFZ strongly inhibits RdRp activity.

Western blot assay

Total cellular proteins were extracted using radio immunoprecipitation assay (RIPA) lysis buffer containing 1 mM phenylmethanesulfonyl fluoride (PMSF) at 4 °C for 10 min. The extracted proteins were separated by 10% SDS-PAGE and transferred to polyvinylidene difluoride (PVDF) membranes. The membranes were blocked with 5% skimmed milk in Tris-buffered saline with Tween 20 (TBST) for 2 h and incubated with primary antibodies for 1 h at room temperature. After washing with TBST, the membranes were incubated with Goat Anti-Mouse IgG-HRP at 37 °C for 45 min. The membranes were washed with TBST and detected using Tanon-5200 multi-infrared imaging system.

RT-qPCR

Total PEDV RNA was extracted from the cells or cell culture supernatants. The *N* mRNA level or viral loads were determined using Hieff® qPCR SYBR Green Master Mix (11201ES03, YEASEN, China) and primers targeting the PEDV *N* gene as described previously (Supplementary Table S2) (Huang et al., 2023b).

Immunofluorescence assay (IFA)

Vero E6 cells were infected with PEDV at an MOI of 0.1. After 10 h of infection, the supernatant was removed, and the cells were fixed with 80% ice-cold ethanol for 45 min at 4 °C. The cells were washed three times with PBS and then mouse anti-PEDV N mAb was added. After being washed with three times with PBS, the cells were incubated with Goat Anti-Mouse IgG AF 488. The fluorescent particles were observed and counted using the Invitrogen EVOS FL Auto Cell Imaging System.

Time-of-addition assay

To identify the stage of viral infection inhibited by CFZ, a time-of-drug-addition assay was performed. Briefly, the cells were infected with PEDV (MOI = 0.1), and CFZ at a concentration of 10 μM was added at different time points before, during, or after PEDV infection: 16h∼10h, −16h∼0h, 0h∼1h, 0h∼2h, 0h∼10h, 1h∼10h, 2h∼10h, and 5h∼10 h. The infected cells were then incubated in a 5% CO_2 incubator at 37 °C after inoculation for 10 h. Supernatant was collected, and RNA was extracted and measured by RT-qPCR. Total cellular proteins were extracted and detected by Western blot. Cells were fixed and detected by IFA assays.

Effects of CFZ on PEDV administrated in different life-cycle stage of virus

To investigate the effects of CFZ on different stages of the PEDV life cycle, the 12-well plates were seeded with Vero E6 cells. For the attachment assay, Vero E6 cells were treated with CFZ (10 μM) or DMSO at 37 °C for 1 h, and then the cells were infected with PEDV (MOI = 0.1) for 15 min and 1 h at 4 °C. The supernatants and cells were collected for $TCID_{50}$ and RT-qPCR analysis, respectively. To determine whether CFZ affects the internalization of PEDV into Vero E6 cells, the cells were infected with 0.1 MOI PEDV at 4 °C for 1 h. After washed twice with PBS to remove the unbound viruses, the supernatant was replaced with DMEM containing CFZ (10 μM) or DMSO, and then incubated at 37 °C for the indicated time (2 hpi, 3 hpi). The cells were then washed with PBS and collected, and the mRNA levels of PEDV N and GAPDH were evaluated by RT-qPCR. The supernatants were collected for $TCID_{50}$ analysis. For the replication assay, Vero E6 cells were inoculated with 0.1 MOI PEDV at 37 °C for 1 h and washed twice with PBS to remove the unbound viruses. At 4 hpi, the culture medium was replaced with fresh DMEM containing CFZ (10 μM) or DMSO. The supernatants and cells were collected at 6, 8, and 10 hpi and measured using $TCID_{50}$ and RT-qPCR, respectively. The cells were fixed and detected by IFA assays, and total cellular proteins were extracted and detected by Western blot. For the release assay, Vero E6 cells were infected with PEDV (0.1 MOI) at 37 °C for 1 h, and the fresh medium was replaced. At 10 hpi, the cells were washed three times and medium was replaced with fresh DMEM containing CFZ (10 μM) or DMSO. The cultures were incubated at 37 °C for the time indicated (0.5, 1, and 2 h), and the supernatant was harvested and quantified by absolute fluorescence quantification.

CoV-RdRp-Gluc reporter assay

HEK-293T cells were plated overnight and transfected with pcaggs-Nsp12-Flag and PEDV-Gluc plasmids using Lipo 8000™ Transfection Reagent (Beyotime, China). At 6 h post-transfection, cells were treated with CFZ or DMSO (control). For the luciferase assay, a 5 mM Coelenterazine-h stock solution was prepared in propylene glycol. The working solution (50 μM) was freshly diluted in PBS and incubated at room temperature for 30 min under light-protected conditions. Luminescence was measured by adding 10 μL of cell supernatant to a white 96-well plate, followed by injection of 60 μL working solution, with immediate reading using a BioTek Synergy2 multimode microplate reader (BioTek, USA).

Determination of direct virion inactivation activity of CFZ

To investigate whether CFZ has an inactivation effect on PEDV, CFZ (10 μM) or DMSO was incubated with PEDV (0.1 MOI) at 37 °C for 15 min, 30 min, 1 h, 3 h and 5 h. The mixture was then placed into Vero E6 cells seeded in 12-well plates for 10 h. The cells were then washed with PBS and the relative expression of the *N* gene were measured using RT-qPCR.

To determine whether CFZ could directly degrade RBD protein (460-640aa), CFZ at a concentration of 10 μM was incubated with 50 μg purified RBD protein for 1 h or 3 h at 37 °C. The mixtures were then analyzed by SDS-PAGE and stained with Coomassie blue dye to observe specific bands.

To further investigate the antiviral effect of CFZ, the morphology of PEDV was analyzed by transmission electron microscopy (TEM) after treatment with 10 μM CFZ or 0.01% Triton X-100 at 37 °C for 3 h. About 4 mL of virus culture medium was collected and centrifuged at 7000 ×*g* and 9000 ×*g*, respectively. The supernatant was centrifuged at 90,000 ×*g* for 3 h. The resultant pellet was suspended in TNE buffer, and 4 μL of the suspension containing virus particles was placed onto a carbon-coated copper grid for 1 min. After staining with 2 % phosphotungstic acid (PTA), the morphology of the virus particles was observed under TEM.

RNA-seq analysis

Virus-infected or mock-infected Vero E6 cells were used for transcriptional analysis. Specifically, the Vero E6 cells were infected with or without PEDV (MOI = 0.1) and treated with CFZ or DMSO for 8h. Total RNA was extracted using Invitrogen Life Technologies'Trizol reagent, and Illumina's NovaSeq 6000 platform was used to perform sequencing after quantifying the Agilent high-sensitivity DNA assay on a Bioanalyzer 2100 system as described previously(Huang et al., 2023b). Finally, genes expression differences, GO enrichment analysis, and KEGG pathway enrichment analysis, were performed by DESeq analysis, hypergeometric distribution method and ClusterProfiler (3.4.4) software, respectively.

Antiviral synergy assay

Different doses of Remdesivir and Molnupiravir were combined with the different doses of CFZ or DMSO to observe the synergistic antiviral effects. Vero E6 cells were infected with PEDV at 0.1 MOI and then treated with CFZ combined with increasing doses of Remdesivir and Molnupiravir. After infection for 10 h, the relative expression of the N gene was quantified by fluorescence quantitative PCR to evaluate the

synergistic antiviral effect. Data were analyzed using SynergyFinder and a summary synergy score was generated (>10 indicates synergistic, −10 to +10 indicates additive, and <−10 indicates antagonistic).

Molecular docking of coronavirus spike and RdRp

Chai-1 is a multi-modal foundation model specifically designed to predict the three-dimensional (3D) structure of biomolecule(team et al., 2024). The 3D structures of PEDV *SHpd2012* spike protein and RdRp were predicted using the Chai-1 online platform (https://lab.chaidiscovery.com/). For this prediction, multiple sequence alignment (MSA) was set to MMseqs2 and the remaining parameters were default. CFZ from the PubChem Compound Database (https://pubchem.ncbi.nlm.nih.gov/) was used for the preparation of ligands to generate 3D conformations (Compound CID: 2794). Molecular docking was performed using CB-Dock2, which integrates the AutoDock Vina v1.1.2 algorithm for ligand-receptor interaction analysis (Liu et al., 2022; Yang et al., 2022). The workflow comprised protein cavity detection to identify five potential ligand-binding pockets per target, followed by automated docking of CFZ. The optimal docking pose was selected according to the lowest Vina score.

FRET-based assays for enzymatic characteristics

For protein expression, PET-28a-Nsp5 plasmids were transformed into *E. coli* BL21 (DE3) and then cultured at 37 °C in LB medium until reaching an OD_{600nm} of 0.6–0.8. Subsequently, protein expression was induced by adding 1 mM isopropyl-β-D-thiogalactopyranoside (IPTG). The peptide Dabcyl-YNSTLQ↓AGLRKM-E-Edans was used as PEDV 3CLpro substrate. Specific operational steps were performed according to previous report (Ye et al., 2016). We used 20 μM and 40 μM concentrations to evaluate the efficacy of CFZ against PEDV 3CLpro.

Statistical analysis

Statistical analysis was performed using GraphPad Prism 9.5.1.733 software and significance was assessed using Student's *t*-test. The asterisks in the figures indicate significant differences (* $P < 0.05$; ** $P < 0.01$; *** $P < 0.001$; ns = not significant).

DATA AVAILABILITY

Data supporting the findings of this study are reported in the main text and figures and in Supplementary figures.

ETHICS STATEMENT

This article does not contain any studies with human or animal subjects performed by any of the authors.

AUTHOR CONTRIBUTIONS

Shuting Zhou: conceptualization, methodology, software, investigation, data curation, validation, writing- original draft, writing-review & editing. Junrui Zhu: methodology, resources, investigation. Houde Zhao: Investigation, Methodology. Zixin Huang: data curation, software, formal analysis. Kangqi Zheng: data curation, validation. Fan Xia: investigation, software, methodology. Yufan Xu: data curation, software, formal analysis. Guocheng Zhao: Software. Jijie Jiang: Software. En Zhang: investigation, data curation. Haoyang Nian: software, formal analysis. Li Cui: resources, writing-review & editing. Tao Sun: writing-review & editing. Xiangfeng Wang: software, formal analysis. Yanjun Zhou: visualization, supervision. Zhibiao Yang: resources, writing-review & editing, supervision. Zhe Wang: conceptualization, resources, project administration, writing -review & editing, supervision, funding acquisition.

CONFLICT OF INTEREST

The authors declare that they have no conflict of interest.

ACKNOWLEDGMENTS

This research was kindly supported by a grant from the National Key Research and Development Plans of China (No. 2021YFD1800401) to Zhe Wang, the National Natural Science Foundation of China (No. 32070128) to Zhe Wang, the Shanghai Biomedical Science and Technology Support Special Project (No. 21S11900200) to Zhe Wang, the National Natural Science Foundation of China (No. 31472211) to Zhi-Biao Yang, the Natural Science Foundation of Shanghai (No. 21ZR1433900) to Zhibiao Yang, the National Key Research and Development Program of China (No. 2022YFD1800805) to Yanjun Zhou, the Pinduoduo-China Agricultural University Research Fund (PC2024A01003) to Xiangfeng Wang, and the Biomedicine and Technology Supporting Project of the Shanghai Science and Technology Innovation Plan (Grant No. 22S11902200, China) to Tao Sun.

We thank Mengyu Yan and Ya Yu, both from Shanghai Jiao Tong University's Instrumental Analysis Center, for their assistance with the Density Gradient Centrifugation system and Transmission Electron Microscopy, respectively. We special thanks to Xinchu Zhou (Shanghai Jiao Tong University School of Agriculture and Biology, Experimental Internship Field Co., Ltd.) and Tianlong Wang (Shanghai Jiao Tong University School of Agriculture and Biology, Experimental Internship Field Co., Ltd.) for experiments. Finally, we thank all members from both the Wang and Yang Labs for their critical discussions and revisions to the document.

APPENDIX A. SUPPLEMENTARY DATA

Supplementary data to this article can be found online at https://doi.org/10.1016/j.virs.2025.05.012.

REFERENCES

Bald, D., Villellas, C., Lu, P., Koul, A., 2017. Targeting energy metabolism in Mycobacterium tuberculosis, a new paradigm in antimycobacterial drug discovery. mBio 8, e00272-17.

Chen, B., Dong, S., Yu, L., Si, F., Li, C., Xie, C., Yu, R., Li, Z., 2023. Three amino acid substitutions in the spike protein enable the coronavirus porcine epidemic diarrhea virus to infect Vero cells. Microbiol. Spectr. 11, e0387222.

Chen, P., Wang, K., Hou, Y., Li, H., Li, X., Yu, L., Jiang, Y., Gao, F., Tong, W., Yu, H., Yang, Z., Tong, G., Zhou, Y., 2019. Genetic evolution analysis and pathogenicity assessment of porcine epidemic diarrhea virus strains circulating in part of China during 2011-2017. Infect. Genet. Evol. 69, 153–165.

Cholo, M.C., Steel, H.C., Fourie, P.B., Germishuizen, W.A., Anderson, R., 2012. Clofazimine: current status and future prospects. J. Antimicrob. Chemother. 67, 290–298.

Chutiwitoonchai, N., Akkarawongsapat, R., Chantawarin, S., Jiarpinitnun, C., Liwnaree, B., Teeravechyan, S., Soodvilai, S., 2025. Antiviral effect of pinostrobin, a bioactive constituent of Boesenbergia rotunda, against porcine epidemic diarrhea virus. Antivir. Res. 234, 106073.

Fernandes, R.S., DE Godoy, A.S., Santos, I.A., Noske, G.D., DE Oliveira, K.I.Z., Gawriljuk, V.O., Gomes Jardim, A.C., Oliva, G., 2021. Discovery of an imidazonaphthyridine and a riminophenazine as potent anti-Zika virus agents through a replicon-based high-throughput screening. Virus Res. 299, 198388.

Guo, S., Zhang, Y., Liu, Z., Wang, D., Liu, H., Li, L., Chen, Q., Yang, D., Liu, Q., Guo, H., Mou, S., Chen, H., Wang, X., 2023. Brincidofovir is a robust replication inhibitor against African swine fever virus in vivo and in vitro. Emerg. Microb. Infect. 12, 2220572.

He, W.T., Bollen, N., Xu, Y., Zhao, J., Dellicour, S., Yan, Z., Gong, W., Zhang, C., Zhang, L., Lu, M., Lai, A., Suchard, M.A., Ji, X., Tu, C., Lemey, P., Baele, G., Su, S., 2022. Phylogeography reveals association between swine trade and the spread of porcine epidemic diarrhea virus in China and across the world. Mol. Biol. Evol. 39, msab364.

Huang, Y., Yang, C., Xu, X.F., Xu, W., Liu, S.W., 2020. Structural and functional properties of SARS-CoV-2 spike protein: potential antivirus drug development for COVID-19. Acta Pharmacol. Sin. 41, 1141–1149.

Huang, Z.X., Zhou, S.T., Wang, J., Yang, Z.B., Wang, Z., 2023a. Remdesivir inhibits Porcine epidemic diarrhea virus infection in vitro. Heliyon 9, e21468.

Huang, Z.X., Zhou, S.T., Yang, Z.B., Wang, Z., 2023b. Molnupiravir inhibits porcine epidemic diarrhea virus infection in vitro. Viruses 15, 1317.

Jiang, L., Gu, M., Xiao, J., Zhao, Y., Shen, F., Guo, X., Li, H., Guo, D., Li, C., Zhu, Q., Yang, D., Xing, X., Sun, D., 2025. Ethyl caffeate as a novel targeted inhibitor of

3CLpro with antiviral activity against porcine epidemic diarrhea virus. Virology (New York, N. Y.) 604, 110406.
Kabinger, F., Stiller, C., Schmitzová, J., Dienemann, C., Kokic, G., Hillen, H.S., HöBARTNER, C., Cramer, P., 2021. Mechanism of molnupiravir-induced SARS-CoV-2 mutagenesis. Nat. Struct. Mol. Biol. 28, 740–746.
Kokic, G., Hillen, H.S., Tegunov, D., Dienemann, C., Seitz, F., Schmitzova, J., Farnung, L., Siewert, A., HöBARTNER, C., Cramer, P., 2021. Mechanism of SARS-CoV-2 polymerase stalling by remdesivir. Nat. Commun. 12, 279.
Leanza, L., O'Reilly, P., Doyle, A., Venturini, E., Zoratti, M., Szegezdi, E., Szabo, I., 2014. Correlation between potassium channel expression and sensitivity to drug-induced cell death in tumor cell lines. Curr. Pharm. Des. 20, 189–200.
Li, C., Huang, J., Yu, Y., Wan, Z., Chiu, M.C., Liu, X., Zhang, S., Cai, J.P., Chu, H., Li, G., Chan, J.F., To, K.K., Yang, Z., Jiang, S., Yuen, K.Y., Clevers, H., Zhou, J., 2023a. Human airway and nasal organoids reveal escalating replicative fitness of SARS-CoV-2 emerging variants. Proc. Natl. Acad. Sci. U. S. A. 120, e2300376120.
Li, C., Li, W., Lucio DE Esesarte, E., Guo, H., VAN Den Elzen, P., Aarts, E., VAN Den Born, E., Rottier, P.J.M., Bosch, B.J., 2017. Cell attachment domains of the porcine epidemic diarrhea virus spike protein are Key targets of neutralizing antibodies. J. Virol. 91, e00273-17.
Li, C., Song, W., Chan, J.F., Chen, Y., Liu, F., Ye, Z., Lam, A.H., Cai, J., Lee, A.C., Wong, B.H., Chu, H., Lung, D.C., Sridhar, S., Chen, H., Zhang, A.J., Yuen, K.Y., 2023b. Intranasal infection by SARS-CoV-2 Omicron variants can induce inflammatory brain damage in newly weaned hamsters. Emerg. Microb. Infect. 12, 2207678.
Li, M., Pan, Y., XI, Y., Wang, M., Zeng, Q., 2023c. Insights and progress on epidemic characteristics, genotyping, and preventive measures of PEDV in China: a review. Microb. Pathog. 181, 106185.
Li, S., Zhu, Z., Yang, F., Cao, W., Yang, J., Ma, C., Zhao, Z., Tian, H., Liu, X., Ma, J., Xiao, S., Zheng, H., 2021. Porcine epidemic diarrhea virus membrane protein interacted with IRF7 to inhibit type I IFN production during viral infection. J. Immunol. 206, 2909–2923.
Li, Z., Ma, Z., Li, Y., Gao, S., Xiao, S., 2020. Porcine epidemic diarrhea virus: molecular mechanisms of attenuation and vaccines. Microb. Pathog. 149, 104553.
Lin, S., Hua, W., Wang, S., Zhang, Y., Chen, X., Liu, H., Shao, L., Chen, J., Zhang, W., 2022. In vitro assessment of 17 antimicrobial agents against clinical Mycobacterium avium complex isolates. BMC Microbiol. 22, 175.
Liu, Y., Yang, X., Gan, J., Chen, S., Xiao, Z.X., Cao, Y., 2022. CB-Dock2: improved protein-ligand blind docking by integrating cavity detection, docking and homologous template fitting. Nucleic Acids Res. 50, W159–w164.
Luo, Y.R., Zhou, S.T., Yang, L., Liu, Y.P., Jiang, S.Y., Dawuli, Y., Hou, Y.X., Zhou, T.X., Yang, Z.B., 2020. Porcine epidemic diarrhoea virus induces cell-cycle arrest through the DNA damage-signalling pathway. J Vet Res 64, 25–32.
Mirnejad, R., Asadi, A., Khoshnood, S., Mirzaei, H., Heidary, M., Fattorini, L., Ghodousi, A., Darban-Sarokhalil, D., 2018. Clofazimine: a useful antibiotic for drug-resistant tuberculosis. Biomed. Pharmacother. 105, 1353–1359.
Peng, Q., Fan, B., Song, X., He, W., Wang, C., Zhao, Y., Guo, W., Zhang, X., Liu, S., Gao, J., Li, K., Zhang, B., Zhou, J., Li, Y., Guo, R., Li, B., 2023. Genetic signatures associated with the virulence of porcine epidemic diarrhea virus AH2012/12. J. Virol. 97, e0106323.
Rashida, Z., L, S., 2021. The pentose phosphate pathway and organization of metabolic networks enabling growth programs. Curr. Opin. Syst. Biol. 28, 100390.
Su, M., Shi, D., Xing, X., Qi, S., Yang, D., Zhang, J., Han, Y., Zhu, Q., Sun, H., Wang, X., Wu, H., Wang, M., Wei, S., Li, C., Guo, D., Feng, L., Sun, D., 2021. Coronavirus porcine epidemic diarrhea virus nucleocapsid protein interacts with p53 to induce cell cycle arrest in S-phase and promotes viral replication. J. Virol. 95, e0018721.
Tang, T., Bidon, M., Jaimes, J.A., Whittaker, G.R., Daniel, S., 2020. Coronavirus membrane fusion mechanism offers a potential target for antiviral development. Antivir. Res. 178, 104792.
Team, C.D., Boitreaud, J., Dent, J., Mcpartlon, M., Meier, J., Reis, V., Rogozhonikov, A., Wu, K., 2024. Chai-1: decoding the molecular interactions of life. bioRxiv, 10.10.615955, 2024.
Wang, D., Ge, X., Chen, D., Li, J., Cai, Y., Deng, J., Zhou, L., Guo, X., Han, J., Yang, H., 2018. The S gene is necessary but not sufficient for the virulence of porcine epidemic diarrhea virus novel variant strain BJ2011C. J. Virol. 92, e00603–e00618.
Wang, K., Xie, C., Zhang, J., Zhang, W., Yang, D., Yu, L., Jiang, Y., Yang, S., Gao, F., Yang, Z., Zhou, Y., Tong, G., 2016. The identification and characterization of two novel epitopes on the nucleocapsid protein of the porcine epidemic diarrhea virus. Sci. Rep. 6, 39010.
Wang, L., Xia, Z., Tang, W., Sun, Y., Wu, Y., Kwok, H.F., Sun, F., Cao, Z., 2022. p38 activation and viral infection. Expet Rev. Mol. Med. 24, e4.
Wang, S., Wang, Z., Li, Y., Tu, S., Zou, J., Cheng, Y., Zhang, H., Suolang, S., Zhou, H., 2023a. Generation of whole-porcine neutralizing antibodies of an alphacoronavirus by single B cell antibody technology. Antivir. Res. 220, 105754.
Wang, X., Lu, L., Jiang, S., 2023b. SARS-CoV-2 Omicron subvariant BA.2.86: limited potential for global spread. Signal Transduct. Targeted Ther. 8, 439.
Wang, Y., Huang, H., Li, D., Zhao, C., Li, S., Qin, P., Li, Y., Yang, X., DU, W., Li, W., Li, Y., 2023c. Identification of niclosamide as a novel antiviral agent against porcine epidemic diarrhea virus infection by targeting viral internalization. Virol. Sin. 38, 296–308.
Wang, Z., Soni, V., Marriner, G., Kaneko, T., Boshoff, H.I.M., Barry 3Rd, C.E., Rhee, K.Y., 2019. Mode-of-action profiling reveals glutamine synthetase as a collateral metabolic vulnerability of M. tuberculosis to bedaquiline. Proc. Natl. Acad. Sci. U. S. A. 116, 19646–19651.
Wu, J., Cao, S., Lei, S., Liu, Q., Li, Y., Yu, Y., Xie, H., Li, Q., Zhao, X., Chen, R., Huang, W., Xiao, X., Yu, Y., Song, D., Li, Y., Wang, Y., 2021. Clofazimine: a promising inhibitor of rabies virus. Front. Pharmacol. 12, 598241.
Wu, Y., Li, M., Tian, J., Yan, H., Pan, Y., Shi, H., Shi, D., Chen, J., Guo, L., Feng, L., 2023. Broad antagonism of coronaviruses nsp5 to evade the host antiviral responses by cleaving POLDIP3. PLoS Pathog. 19, e1011702.
Xie, Y., Guo, X., Hu, T., Wei, D., Ma, X., Wu, J., Huang, B., Shen, J., 2021. Significant inhibition of porcine epidemic diarrhea virus in vitro by remdesivir, its parent nucleoside and β-D-N(4)-hydroxycytidine. Virol. Sin. 36, 997–1005.
Xu, Q., Wang, F., Jiao, W., Zhang, M., Xing, G., Feng, H., Sun, X., Hu, M., Zhang, G., 2023. Virtual screening-based peptides targeting spike protein to inhibit porcine epidemic diarrhea virus (PEDV) infection. Viruses 15, 381.
Yang, S., Huang, X., Li, S., Wang, C., Jansen, C.A., Savelkoul, H.F.J., Liu, G., 2023. Linoleic acid: a natural feed compound against porcine epidemic diarrhea disease. J. Virol. 97, e0170023.
Yang, X., Liu, Y., Gan, J., Xiao, Z.X., Cao, Y., 2022. FitDock: protein-ligand docking by template fitting. Briefings Bioinf. 23, bbac087.
Ye, G., Deng, F., Shen, Z., Luo, R., Zhao, L., Xiao, S., Fu, Z.F., Peng, G., 2016. Structural basis for the dimerization and substrate recognition specificity of porcine epidemic diarrhea virus 3C-like protease. Virology (New York, N. Y.) 494, 225–235.
Yuan, S., Yin, X., Meng, X., Chan, J.F., Ye, Z.W., Riva, L., Pache, L., Chan, C.C., Lai, P.M., Chan, C.C., Poon, V.K., Lee, A.C., Matsunaga, N., Pu, Y., Yuen, C.K., Cao, J., Liang, R., Tang, K., Sheng, L., DU, Y., Xu, W., Lau, C.Y., Sit, K.Y., Au, W.K., Wang, R., Zhang, Y.Y., Tang, Y.D., Clausen, T.M., Pihl, J., Oh, J., Sze, K.H., Zhang, A.J., Chu, H., Kok, K.H., Wang, D., Cai, X.H., Esko, J.D., Hung, I.F., Li, R.A., Chen, H., Sun, H., Jin, D.Y., Sun, R., Chanda, S.K., Yuen, K.Y., 2021. Clofazimine broadly inhibits coronaviruses including SARS-CoV-2. Nature 593, 418–423.
Zhai, X., Kong, N., Zhang, Y., Song, Y., Qin, W., Yang, X., Ye, C., Ye, M., Tong, W., Liu, C., Zheng, H., Yu, H., Zhang, W., Yang, X., Zhang, G., Tong, G., Shan, T., 2023. N protein of PEDV plays chess game with host proteins by selective autophagy. Autophagy 19, 2338–2352.
Zhang, H., Zou, C., Peng, O., Ashraf, U., Xu, Q., Gong, L., Fan, B., Zhang, Y., Xu, Z., Xue, C., Wei, X., Zhou, Q., Tian, X., Shen, H., Li, B., Zhang, X., Cao, Y., 2023. Global dynamics of porcine enteric coronavirus PEDV epidemiology, evolution, and transmission. Mol. Biol. Evol. 40, msad052.
Zhang, S., Cao, Y., Yang, Q., 2020. Transferrin receptor 1 levels at the cell surface influence the susceptibility of newborn piglets to PEDV infection. PLoS Pathog. 16, e1008682.
Zhang, S., Shi, W., Feng, J., Zhang, W., Zhang, Y., 2017. Varying effects of common tuberculosis drugs on enhancing clofazimine activity in vitro. Emerg. Microb. Infect. 6, e28.